Ultra-compact variable optical attenuator based on slow light photonic crystal waveguide

Qiang Zhao (赵 强), Kaiyu Cui (崔开宇)*, Xue Feng (冯 雪), Yidong Huang (黄翊东), Yongzhuo Li (李永卓), Dengke Zhang (张登科), and Wei Zhang (张 巍)

Department of Electronic Engineering, Tsinghua University, Beijing 100084, China

**Corresponding author: kaiyucui@tsinghua.edu.cn*

Received July 27, 2012; accepted October 10, 2012; posted online January 30, 2013

An ultra-compact variable optical attenuator based on slow light photonic crystal waveguide with thermo-optic effect is demonstrated. Along with power consumption of as low as 30.7 mW, a variable attenuation range of 10 dB is experimentally achieved by shifting the transmission spectrum at about 4.6 nm. The length of the proposed device is only 20 μm.

OCIS codes: 130.0130, 230.0230, 250.0250.

doi: 10.3788/COL201311.031301.

Photonic crystal waveguides (PCWGs) located within high contrast slabs have attracted a great deal of attention due to their unique properties, such as the photonic band gap and the slow light effect. High contrast slabs can be used to enhance the interaction between light and matter in PCWGs, thereby reducing the size of the device[1,2]. This development is very significant in realizing compact functional devices for photonic integrated circuits (PICs). Variable optical attenuators (VOAs) are essential devices for PICs that employ the wavelength-division multiplexing system. The typical on-chip VOAs are implemented by micro-electro-mechanical systems (MEMSs)[3,4] or planar lightwave circuits (PLCs)[5−7]. However, both kinds of VOAs usually have millimeter-level sizes that are difficult to integrate in PICs[3,7]. Thus, small VOAs for PIC applications must be further developed. Through the introduction of silicon PCWGs, compact VOAs can now be realized by tuning the output optical power, and this function can be achieved in three ways. The most common approach is achieved through the Mach-Zender interferometer (MZI) structure. Vlasov *et al.* experimentally demonstrated a doped silicon PCWG optical modulator with a MZI structure and an electric controlled heater[8]. Gu *et al.*[9,10] demonstrated PCWG modulators with metal microheaters applied to either arm of the MZI. However, the main drawback of the MZI structure is its large device size, which hampers the realization of the π phase-shift. The shortest device length that has been reported is 80 μm[10]. Apart from the MZI structure, the tunable PCWG directional coupler can also be used to achieve the VOA function[11]. However, a complex structure design is needed for this type of PCWG directional coupler. The third way is to utilize the cutoff effect of a single PCWG, which provides a simple platform for compact devices with less complex structure designs. Tinker *et al.*[12,13] theoretically analyzed the realization of the tunable single PCWG by thermo-optical effect, demonstrating a PCWG modulator with the cutoff effect. Wang *et al.* theoretically modeled the mechanism of the cutoff effect to realize a switch using a single PCWG[14]. Based on the theoretical studies above, compact VOAs with reduced power consumption can be realized with the slow light PCWG. However, no experimental research has yet to be reported.

In this letter, we first employ the cutoff effect in slow light PCWG to realize ultra-compact thermo-optic VOAs. Then, we experimentally study the performance of such novel VOAs. A variable attenuation range of 10 dB is achieved using a PCWG (length: 20 μm) with an integrated Al microheater. The maximum tuning voltage and power consumption are as low as 0.35 V and 30.7 mW, respectively, which match our theoretical prediction. This promising result shows the potential of slow light PCWG VOA for on-chip applications in future PICs.

We formed the structure of the proposed VOA by a W1 PCWG and an Al microheater, which was used for tuning the temperature of the PCWG. The schematic of the device is shown in Fig. 1(a), in which the W1 PCWG serves as a line-defect waveguide by taking one row of the holes away from the triangular lattice photonic crystal. The W1 PCWG was fabricated on a silicon-on-insulator (SOI) substrate by electron beam lithography and inductively coupled plasma dry etching. The SOI substrate has a silicon slab on top and a buried SiO_2 layer with thicknesses of 220 nm and 3 μm, respectively. Figure 1(b) shows the scanning electron microscope (SEM) image of the fabricated W1 PCWG[15]. The lattice constant of the PCWG and the radius of the hole are 0.395 and 0.11 μm, respectively. SiO_2 cladding layer with a thickness of 1 μm was deposited on the surface by plasma-enhanced chemical vapor deposition. This dioxide layer forms a vertical symmetric structure to improve the coupling efficiency between fiber and access waveguide and performs as an isolated layer to prevent the absorption loss of the microheater[9]. On top of the SiO_2 cladding layer, the Al strip microheater (width: 4.7 μm, thickness: 250 nm, length: 20 μm) was deposited by metal evaporation and one-step lift-off after ultraviolet (UV) lithography. The deposited position was located over the PCWG in order to achieve high heating efficiency. However, limited by the fabrication precision, a 2-μm deviation from the center of the PCWG can be found in the fabricated device (Fig. 1(b)). Finally, we

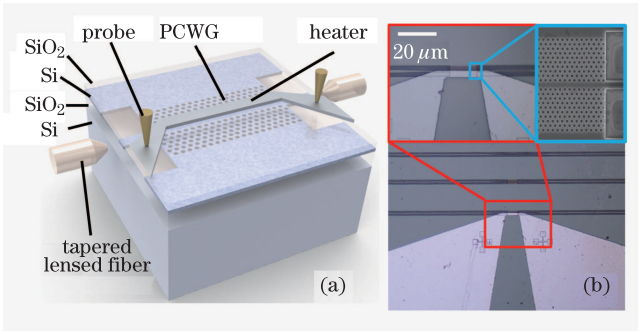

Fig. 1. (a) Schematic of the VOA structure. (b) SEM image for the fabricated W1 PCWG and microscope image of the W1 PCWG with input and output waveguides and Al microheater.

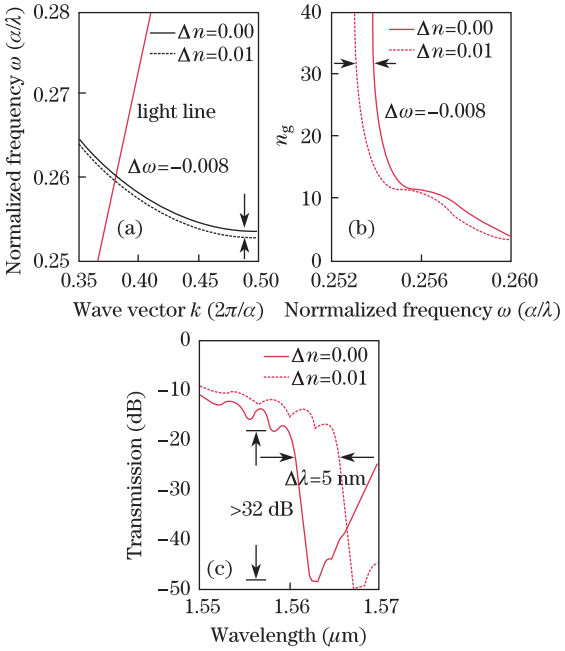

Fig. 2. Simulation results for (a) dispersion curve, (b) group indices, and (c) transmission spectra of the fundamental mode in the W1 PCWG with different refractive index variations $\Delta n = 0$ and $\Delta n = 0.01$.

ground the wafer to a thickness of 100 μm and cleaved it into samples with a length of about 1.5 mm for measurement.

The band structure and transmission spectra of the transverse electric (TE) mode of the W1 PCWG were calculated by two-dimensional (2D) plane wave expansion (PWE) method and 2D finite-difference time-domain (FDTD) method with an effective refractive index $n_{\rm eff}$=2.74. Here, $n_{\rm eff}$ can be determined by the thickness of the fabricated photonic crystal slab and by the vertical refractive index distribution; its validity is further confirmed by experimental results of the transmission spectra, which fit well with the simulation ones. Figures 2(a) and (b) show the dispersion curve and group index $n_{\rm g}$ (inversely proportional to group velocity) of the fundamental mode with different refractive index variations (Δn), respectively. The cutoff frequency of the fundamental mode changes with the variation of the refractive index, and this can be dynamically controlled by tuning the heating temperature of the microheater based on our previous work[16−18]. The variation of the refractive index tuned by the heating temperature can be calculated using the thermo-optical coefficient of $\Delta n/\Delta T = 1.86 \times 10^{-4} \cdot {\rm K}^{-1}$. The refractive index change of the silicon layer causes the cutoff frequency of the fundamental mode to shift, which also changes the transmission power. A change in the refractive index of $\Delta n = 0.01$ causes an approximately 5 nm red-shift of the cutoff wavelength in the transmission spectra (Fig. 2(c)). This red shift can realize a 32-dB tunable range of the transmission power at around 1 563 nm, which is in the slow light region of the PCWG. The proposed device is polarization-dependent, because the VOA functionality is realized by the band gap of the W1 PCWG obtained only under TE mode polarization.

Steady-state thermal analysis was performed to assess the thermal performance of the proposed VOA. We used the three-dimensional (3D) finite element method (FEM) to model the temperature distribution and power consumption of the device. The thermal simulation model structure followed the same parameters of the previously described VOA (Fig. 3(a), inset). The size of the 3D simulation region was fixed at 100 × 100 × 50 (μm) to ensure a room-temperature boundary condition valid at the bottom of the device. Other boundaries were set to be adiabatic. Different heating temperatures were obtained by changing the bias voltage applied on the microheater. Here, the resistance changing of Al microheater at different temperatures was considered in the thermal model.

Based on this 3D FEM model, we obtained the temperature distribution located just below the microheater in the vertical direction of the proposed VOA (Fig. 3(a)). The black solid and dash curves present the vertical temperature distributions below the strip-type microheater at the center of the PCWG and at a 2-μm deviation from the center, respectively.

The vertical temperature distribution for the case, in which the whole chip surface is covered by the heater, is also given in Fig. 3(a) with the red dotted curve. The slopes of the two parts are similar in the red curve and different in the black curves. This is because the heat conduction varies under different microheater shapes in the form of temperature distribution. In the case of the fully covered microheater, the heat flux simply transfers vertically down to the bottom, no matter above or under the silicon layer, so that the slope is almost the same in several micrometers. On one hand, for the strip-type microheater, the heat flux above the silicon layer transfers downwards to the bottom and spreads horizontally. As such, the temperature falls down more rapidly in the top SiO_2 than in the fully covered type; this corresponds to a smaller slope of the solid line above the silicon layer compared with that of the dotted line. On the other hand, the condition of the thermal boundary was set at the room temperature (300 K) at the device bottom in our simulation. Thus, the temperature changes from a smaller value to the room temperature, causing a larger slope of the solid line under the PCWG layer. Based on the two points, the solid line in the top SiO_2 has a much smaller slope than the bottom part in the case of strip-microheater.

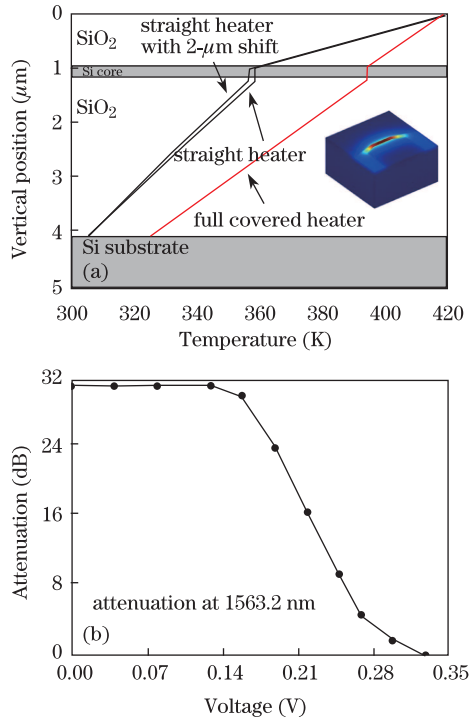

Fig. 3. (Color online) (a) Calculated vertical temperature distributions located below the microheater (black short dash line), 2-μm deviation from the center (black solid line), and the full covered heater (red solid line). The inset is the 3D FEM simulation result for the microheater thermal model. (b) Simulated attenuation characteristic of the VOA at different bias voltages.

Next, we considered the microheater deviation of our fabricated device and evaluated its influence. In the center-located strip-type case (black short dash curve), when the temperature shift in the microheater is 120 K, the temperature shift in the PCWG is 58 K. In contrast, the 2-μm location deviation of the microheater (black solid curve) causes a temperature decrease of 2 K. Compared with the temperature shift of 58 K in the PCWG, this deviation of the microheater in our fabricated device does not affect the power consumption severely. Furthermore, the difference in temperature of the PCWG is just 0.066 K in the vertical direction, and the refractive index change is as small as 1.2×10^{-5}, which is far less than the total refractive index change of the PCWG. This result implies that the temperature distribution in the PCWG layer can be treated as uniform in the vertical direction. Therefore, we can define a heating efficiency ($\Delta T_{\mathrm{PCWG}}/\Delta T_{\mathrm{Heater}}$) as the ratio of the temperature variation for the PCWG region to that for the microheater. Accordingly, the heating efficiencies of the fully covered heater and the microheater with a length of 20 μm are 79% and 45%, respectively[19]. The higher heating efficiency of the fully covered microheater can be attributed to the fact that the heat flux just transfers vertically down to the bottom without spreading horizontally. However, a large covered area of the heater results in huge power consumption.

The simulated attenuation characteristic of the VOA in 1 563.2 nm is shown in Fig. 3(b). A uniform refractive index change was used to calculate the cutoff wavelength shifts by 2D FDTD method, and this was facilitated by the small temperature difference of the silicon layer. A variable attenuation range of 32 dB can be obtained by PCWG with a length of $50a$ when the bias voltage is tuned from 0 to 0.34 V. The maximum operating power consumption was set to 29.8 mW during the simulation.

The experimental transmission spectra and the attenuation characteristics are given in Fig. 4. These were measured using auto-alignment coupling systems. Here, a tunable laser with tuning range from 1 350 to 1 630 nm was used, and the TE polarization mode was fixed by a polarization controller. In addition, two single-mode tapered lens fibers were used to couple the light input as well as to output the VOA. The output power was collected by a photo detector, which was connected to the output tapered lens fiber. Figure 4(a) shows the transmission spectra through the PCWG under different direct current (DC) biases. The measured cutoff wavelength of the W1 PCWG is around 1 565 nm. The spectra show that the cutoff wavelength has a 4.6-nm red-shift when the bias of the microheater increases from 0 to 0.35 V. Accordingly, the attenuation at 1 564.6 nm has a variable range between 0 and 10 dB (Fig. 4(b)). The measured electric resistance of the micro-heater is 4 Ω, which corresponds to the maximum power consumption of as low as 30.7 mW for realizing the 10 dB attenuation.

Next, we determined the variable attenuation range using the slope of the transmission spectra and the temperature variation range of W1 PCWGs. Compared with the simulation results shown in Fig. 2(c), the slope of the transmission curve at the cutoff wavelength measured in the W1 PCWG is smaller, which can be attributed to the fabrication accuracy limitation. The fabrication accuracy of the PCWG is limited to about 10 to 20 nm; this can lead to an imperfect PCWG structure, as in the

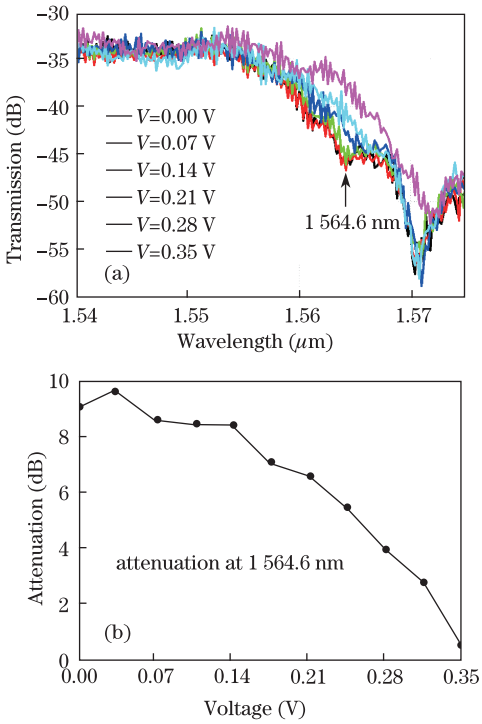

Fig. 4. Experimental results for (a) the transmission spectra of W1 PCWG under different bias voltages from 0 to 0.35 V and (b) attenuation characteristic of the device at the transmission wavelength of 1 564.6 nm.

case in which a small platform appears at around 1 565 nm (Fig. 4(a)), This small platform limits the range of the VOA to only 10 dB. If better fabrication quality is achieved and no platform appears, the transmission loss can increase monotonically, and a 20 dB range (or larger) can be achieved.

Furthermore, we measured the response time by alternating current (AC) modulation. The rise time for this VOA is (35.0±5.0) μs and fall time is (40.0±5.0) μs, which is far faster than the VOAs based on MEMs or PLC[4,6,7].

In conclusion, we demonstrate an ultra-compact on-chip VOA by introducing a slow light W1 PCWG with an integrated Al microheater. By dynamically tuning the temperature of the W1 PCWG, a 4.6-nm red-shift in the transmission spectra is measured and a 10-dB variable attenuation range is obtained while the device length is only 20 μm. The maximum tuning voltage and power consumption are as low as 0.35 V and 30.7 mW, respectively, demonstrating the potential of slow light PCWG VOA for on-chip applications in future PICs.

This work was supported by the National "973" Program of China (Nos. 2011CBA00608, 2011CBA00303, and 2010CB327405), the National Natural Science Foundation of China (Nos. 61036011 and 61036010), and the China Postdoctoral Science Foundation and the National Quality Inspection Service Industry Scientific Research of China (No. 201010007). The authors would also like to thank Dr. Fang Liu, Gengyan Zhang, Xuejian Zhang, and Deyu He for the technical discussions they initiated.

References

1. T. Baba, Nat. Photon. **2,** 465 (2008).
2. S. A. Schulz, L. O'Faolain, D. M. Beggs, T. P. White, A. Melloni, and T. F. Krauss, J. Opt. **12,** 104004 (2010).
3. C. Lee, F. L. Hsiao, T. Kobayashi, K. H. Koh, P. V. Ramana, W. F. Xiang, B. Yang, C. W. Yan, and D. Pinjala, IEEE J. Sel. Top. Quantum **15,** 1529 (2009).
4. X. M. Zhang, A. Q. Liu, C. Lu, and D. Y. Tang, Electron. Lett. **38,** 382 (2002).
5. S. M. Garner and S. Caracci, IEEE Photon. Technol. Lett. **14,** 1560 (2002).
6. X. Q. Jiang, Qi. W, H. Zhang, Y. Tang, Y. L. Hao, J. Y. Yang, and M. H. Wang, IEEE Photon. Technol. Lett. **18,** 610 (2006).
7. D. X. Li, Y. W. Zhang, L. Y. Liu, and L. Xu, Opt. Express **14,** 6029 (2006).
8. Y. A. Vlasov, M. O'Boyle, H. F. Hamann, and S. J. McNab, Nature **438,** 65 (2005).
9. L. L. Gu, W. Jiang, X. N. Chen, and R. T. Chen, IEEE Photon. Technol. Lett. **19,** 342 (2007).
10. T. Chu, H. Yamada, S. Ishida, and Y. Arakawa, IEEE Photon. Technol. Lett. **17,** 2083 (2005).
11. D. M. Beggs, T. P.White, L. Cairns, L. O'Faolain, and T. F. Krauss, Phys. E **41,** 1111 (2009).
12. M. T. Tinker and J. B. Lee, Opt. Express **13,** 7174 (2005).
13. Y. H. Cui, K. Liu, D. L. MacFarlane, and J. B. Lee, Opt. Lett. **35,** 3613 (2010).
14. X. Wang, S. Chakravarty, B. S. Lee, C. Lin, and R. T. Chen, Opt. Lett. **34,** 3202 (2009).
15. Y. Huang, X. Mao, K. Cui, C. Zhang, L. Cao, W. Zhang, and J. Peng, Chin. Opt. Lett. **6,** 704 (2008).
16. K. Cui, Y. Huang, G. Zhang, Y. Li, X. Tang, X. Mao, Q. Zhao, W. Zhang, and J. Peng, Appl. Phys. Lett. **95,** 191901 (2009).
17. K. Cui, Q. Zhao, X. Feng, Y. Huang, Y. Li, D. Wang, and W. Zhang, Appl. Phys. Lett. **100,** 201102 (2012).
18. K. Cui, X. Feng, Y. Huang, Q. Zhang, Z. Hang, and W. Zhang, Appl. Phys. Lett. **101,** 15110 (2012).
19. F. Gan, T. Barwicz, M. A. Popovic, M. S. Dahlem, C. W. Holzwarth, P. T. Rakith, H. I. Smith, E. P. Ippen, and F. X. Kartner, in *Proceedings of Photonics in Switching* 67 (2007).